Hyperelastic Swelling of Stiff Hydrogels

Jing Wang and Justin C. Burton*
Department of Physics, Emory University, 400 Dowman Drive, Atlanta, Georgia 30322, USA

(Received 27 June 2024; revised 30 December 2024; accepted 12 March 2025; published 9 April 2025)

Hydrogels are swollen polymer networks where elastic deformation is coupled to nanoscale fluid flow. As a consequence, hydrogels can withstand large strains and exhibit nonlinear, hyperelastic properties. Previous studies have shown that low-modulus hydrogels and semiflexible biopolymer networks universally contract when sheared on timescales much longer than the poroelastic relaxation timescale. Using rheological and tribological measurements, we find that stiff polyacrylamide and polyacrylic acid hydrogels, with moduli of order ∼10–100 kPa, exclusively swell (dilate) when sheared. Poroelastic relaxation was examined using strain-controlled compression, indicating a volumetric diffusion constant of order 10^{-9} m^2/s. Upon shearing, we observed an increase in normal stress that varied quadratically with shear strain, which persisted for hours. Moreover, we show that this dilatant behavior manifests as swelling during tribological sliding, imbibing the hydrogel with fluid. We suggest that this inherent, hyperelastic dilatancy is an important feature in all stiff hydrogels, and may explain rehydration and mechanical rejuvenation in biological tissues such as cartilage.

DOI: 10.1103/PhysRevLett.134.148203

Introduction—Hydrogels exhibit complex, time-dependent mechanical properties due to their biphasic nature. Material deformation inherently requires the solvent to flow relative to the underlying cross-linked polymer matrix. In recent years, hydrogels have been engineered and investigated for applications such as urban farming [1], cosmetic care [2,3], tissue engineering [4,5], and drug delivery [6–8]. In particular, stiff hydrogels with a Young's modulus >10 kPa exhibit ultralow friction and have been used as a model for articular and artificial cartilage [9–16], including therapeutic, *in vivo* injections for cartilage repair [17,18]. Recent tribological experiments show an increase of cartilage (hydrogel) volume upon sliding at a smooth interface, a process attributed to "tribological rehydration" [19–24]. The rehydration process is velocity-dependent and is claimed to only occur at the hydrogel contact interface as a result of elastohydrodynamic lubrication pressure [25]. In this sense, the application of shear (through mechanical motion, i.e., joint activity) will imbibe the cartilage with fluid, softening and rejuvenating the tissue.

Alternatively, here we will show that rejuvenation and swelling of stiff hydrogels can be ascribed to their bulk, hyperelastic mechanical properties. Specifically, swelling is due to the Poynting effect, which is a second-order elastic effect characterizing stress perpendicular to the direction of shear [26–28]. Examples of the Poynting effect include rubber [29], metal wires [26], soft fiber materials [30,31], soft polymer gels [32,33], and emulsions [34]. The change in normal stress, $\Delta\sigma_N$, in hyperelastic materials is captured by the Mooney-Rivlin model [35,36], which predicts that when sheared at a fixed volume, $\Delta\sigma_N \propto \gamma^2$, where γ is the shear strain. The effect can be positive (dilatant) or negative (contractile). In 2007, Janmey *et al.* [37] first reported contractile behavior in semiflexible biopolymer gels such as fibrin, which has been confirmed by subsequent studies [38–41]. However, Janmey *et al.* [37] also reported a dilatant behavior in low-modulus, weakly cross-linked polyacrylamide (PAAm) hydrogels. While this was attributed to the flexibility of the polymers, instead de Cagny *et al.* [42] revealed that poroelastic flow on long timescales can alter the sign of the normal stress response, so that an initial dilatant behavior can transition to a contractile one in PAAm with moduli of order ∼100 Pa. They further suggested that any confined hydrogel would eventually exhibit negative normal stress in response to shear after sufficient waiting time. However, here we show stiff hydrogels with moduli of order 10–100 kPa *always* exhibit dilatant, hyperelastic behavior, even long after reaching poroelastic equilibrium.

Both contractile and dilatant responses in hydrogels can be predicted based on the change in shear modulus under compression. Following Tighe *et al.* [43,44], when sheared under constant volume, the normal stress response of an elastic solid can be expressed as

$$\Delta\sigma_N = \frac{1}{2} R_v \gamma^2 + \mathcal{O}(\gamma^4), \tag{1}$$

where R_v is the Reynolds coefficient at a fixed volume,

$$R_v = E\left(\frac{\partial G}{\partial \sigma_N}\right)_\gamma - G. \tag{2}$$

*Contact author: justin.c.burton@emory.edu

Here, G is the shear modulus, E is the Young's modulus, and the subscript γ implies that the derivative is taken at constant, infinitesimal shear strain. Generally, $G < E$, and the material will exhibit dilatant behavior if the differential in the first term is large enough and positive. For granular packings, $\partial G/\partial\sigma_N > 0$, as evidenced by studies of dilatancy in granular materials dating back to 1886 [45], and more recently in a broader class of granular materials such as emulsions [34]. For spring networks, often used as a minimal model for cross-linked gels, $\partial G/\partial\sigma_N < 0$, implying that spring networks universally contract upon compression [44,46]. Contractile behavior is indeed observed in semiflexible biopolymer networks and weakly cross-linked hydrogels [37,42]. Conversely, tough and stiff hydrogels are widely used in fundamental and applied science and are promising candidates for cartilage tissue engineering [47–50], yet their hyperelastic behavior remains largely unexplored.

We have conducted a series of both surface tribological sliding and bulk rheological shearing experiments using stiff PAAm and polyacrylic acid (PAA) hydrogels. These hydrogels exclusively dilate in all experiments, in contrast to low-modulus gels and the expected behavior of network materials. We first characterized the volumetric diffusion of the hydrogel network upon compression in order to isolate transient relaxation behavior from rheological response. We then illustrate how dilatant behavior is manifested in confined and unconfined tribological sliding experiments. Finally, we used oscillatory shear and strain sweep to directly measure R_v, and show that Eq. (2), which is derived from a purely elastic solid, is a reasonable estimate to the dilatant behavior. These results provide a natural explanation for the volumetric expansion of cartilage during sliding, and are applicable to a broader class of stiff synthetic hydrogels and biological tissues.

Diffusion-driven relaxation—The hyperelastic response of hydrogels can change in both magnitude and sign during poroelastic relaxation [42]. This process is driven by the relative diffusion of the solvent and polymer network, as described by Doi *et al.* [51,52]. The diffusion constant can be written as

$$D = \frac{Ek(1-\nu)}{\mu(1+\nu)(1-2\nu)}, \tag{3}$$

where E is the Young's modulus of the hydrogel, k is the permeability, μ is the viscosity of the solvent (water), and ν is Poisson's ratio [53]. We note that D does not represent mass diffusion, but rather diffusion of volumetric strain, $\nabla\cdot\vec{\mathbf{u}}$, where $\vec{\mathbf{u}}$ is the displacement field [51]. For the PAAm and PAA hydrogel spheres used in our experiments, $E \approx 35.7$ kPa (Fig. S2) [54], $\nu \approx 0.40$, and $k \propto \xi^2$, where $\xi \approx 5$–15 nm is the mesh size of the polymer network [55]. Thus we expect $D \approx 2 - 20 \times 10^{-9}$ m^2/s. A full description of the hydrogel preparation methods can be found in Supplemental Material (SM) [54].

We characterized the diffusion process in our hydrogels by examining the relaxation of the normal force under compression using a rheometer (AR 2000, TA Instruments). With a 60-mm parallel plate geometry, hydrogel spheres were compressed on top of a plano-concave lens fully immersed in a water bath [Fig. 1(b) inset]. A custom solvent trap was placed on top of the water bath to prevent evaporation over day-long timescales. Each experiment began by applying a constant normal force, F_0, that determined the amount of compressive normal strain ($\approx 1\% - 10\%$). We subsequently recorded the normal force response, $F_N(t)$, during relaxation for 14 h. The normal strain (determined by the rheometer gap

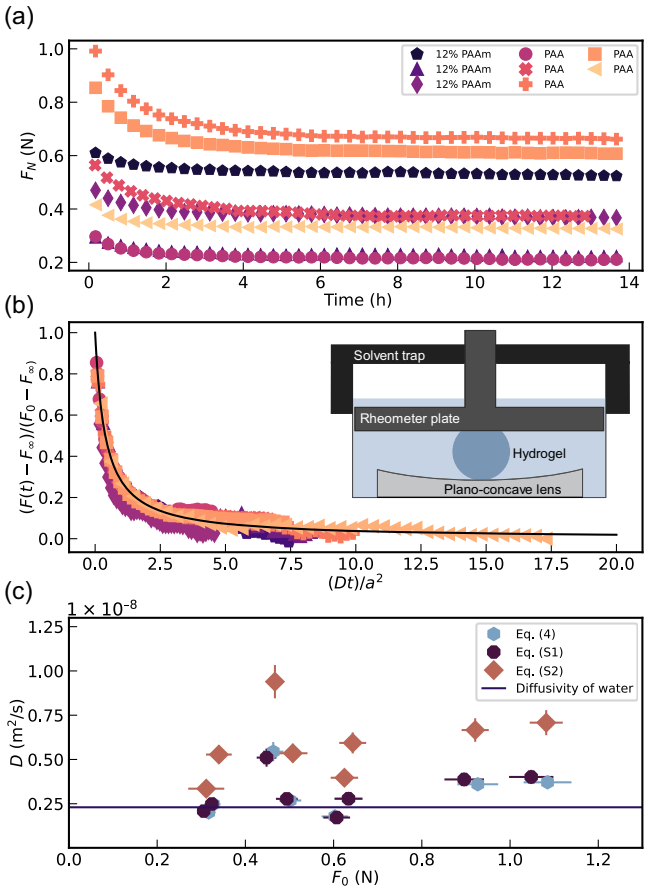

FIG. 1. Stiff hydrogels display poroelastic relaxation upon compression. (a) Under fixed strain, the applied normal force relaxed to a constant value after many hours. (b) Assuming a diffusive relaxation process [Eq. (4) and SM Eqs. (S1) and (S2)], the data can be collapsed by scaling both axes. Inset: experimental schematic showing a hydrogel sphere (diameter $\approx$1.5 cm) compressed in a rheometer and left to relax under constant normal strain. The concave lens ensured centering of the gel. (c) The extracted diffusion constant was independent of the exact fitting form and comparable to, or larger than, the self-diffusivity of water (solid line). Error bars represent 10% for D and 5% for F_0, which comes from variations in the number of fitted data points.

size) remained constant during the experiment. Figure 1(a) shows $F_N(t)$ for commercial PAA and 12% PAAm spheres with different levels of initial compression. In all cases, $F_N(t)$ decreased rapidly at early times but eventually reached a plateau at late times. This behavior agrees with numerous previous studies using indentation methods such as the atomic force microscopy to study hydrogel poroelasticity [19,56–60].

The data in Fig. 1(a) can be collapsed onto a single curve by scaling the vertical and horizontal axes. The initial and final values of the force determine the vertical axis scaling, whereas time is scaled by $\tau = a^2/D$, where D should be the diffusion constant [Eq. (3)]. The contact area a was measured using particle exclusion microscopy [55]. Analytical solutions of simple diffusion problems often consist of an infinite sum of functions with the form $F(t) = \sum f_n(Dt/L^2)$, where L is a characteristic length scale, and the sum runs over n [61]. As such, we should not expect a single functional form to describe our data, but we found good fits with 3–4 parameters. First, to collapse the data in Fig. 1(a), we used the following empirical function, taken from Berry *et al.* [56,57],

$$\frac{F_N(t) - F_\infty}{F_0 - F_\infty} = 1 - \frac{2.56(Dt/a^2)^{0.94}}{1 + 2.56(Dt/a^2)^{0.94}}, \tag{4}$$

where $F_\infty = F_N(t = \infty)$. Since a is measured by microscopy, the fitting parameters were D, F_0, and F_∞. Other fitting functions, such as a stretched exponential with four parameters, provided similar results, as described in SM [54]. The collapsed data is shown in Fig. 1(b). The extracted diffusion constants (D) using Eqs. (4), (S1), and (S2) are shown in Fig. 1(c) as a function of the initial compressive force, F_0. The values of D ranged from $1.8 - 9.4 \times 10^{-9}\,\mathrm{m}^2/\mathrm{s}$, which is consistent with the estimate from Eq. (3), and agrees well with values of D extracted from swelling experiments of similar-sized hydrogel particles [53]. We note that diffusion is relatively fast in stiffer hydrogels since the timescale is inversely proportional to D. For example, in our experiments, $\tau \approx 1$ h, yet in soft gels where $G \approx 100$ Pa, $\tau \approx 15$ h when diffusing over similar millimetric length scales [42].

Tribological swelling—Under constant normal load, stiff hydrogels are free to swell in response to an imposed shear stress, for example, frictional sliding against a smooth surface. The shear stress applied at the sliding interface is transmitted into the bulk, resulting in hyperelastic swelling. In confined environments where swelling is inhibited, this effect manifests as an increase in normal stress. In fully relaxed, compressed hydrogel spheres, we observed sliding-induced swelling using stress-controlled tribology experiments and strain-controlled rheology experiments.

The Fig. 2(a) inset shows our custom-built tribometer [55,62]. Hydrogel spheres were compressed onto an acrylic surface with a constant normal load of $F_N = 0.2$ N. An ink

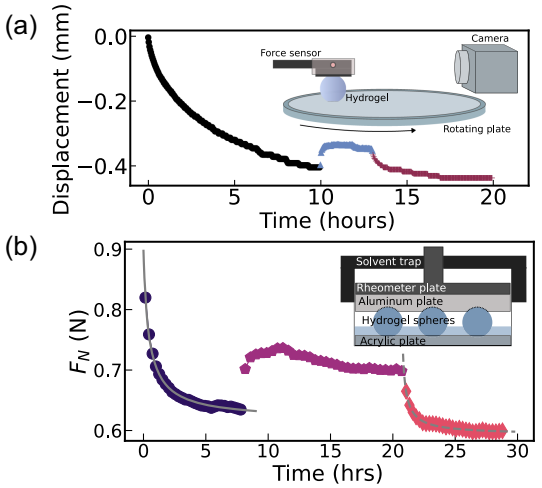

FIG. 2. (a) Stiff hydrogels swell during tribological sliding. Plotted data represents vertical displacement vs time during the initial compression ($t < 10$ h), during sliding at 1.0 cm/s($10\ \mathrm{h} < t < 13$ h), and postsliding ($t > 13$ h). The contact radius of the PAA sphere was ≈3 mm under a normal load of 0.2 N. The inset shows an illustration of the stress-controlled tribology setup for displacement imaging. The relaxation and swelling of the hydrogel was monitored by tracking the vertical position of the pink circle. A thin layer of water was used to ensure hydration of hydrogel spheres. (b) Stiff hydrogels exhibit a positive normal force upon sliding under confinement. The PAA spheres underwent an 8-h initial relaxation, a period of sliding at a constant sliding velocity (0.3 cm/s), and further relaxation postsliding. The solid and dashed gray lines are fits to Eq. (4) with $D = 5.0 \times 10^{-9}\,\mathrm{m}^2/\mathrm{s}$ and $D = 4.7 \times 10^{-9}\,\mathrm{m}^2/\mathrm{s}$, respectively, with a similar fitting error as Fig. 1(c). The inset shows the experimental setup, as described in the main text. Hydrogels were surrounded by a thin layer of water to ensure hydration.

spot was marked on the aluminum fixture that held the hydrogel sphere in place. The spot's vertical position was recorded at 1 fps and tracked using image analysis. The time evolution of the vertical displacement is depicted in Fig. 2(a). We define $t = 0$ h when the normal load was first applied to the hydrogel sphere. For $0 < t < 10$ h, displacement creep was observed, similar to the normal force relaxation in Fig. 1(a). At $t = 10$ h, a constant sliding velocity of 1 cm/s was applied for 3 h. The vertical displacement increased rapidly by 70 μm and ultimately reached a plateau. Importantly, upon cessation of sliding at $t = 13$ h, the vertical displacement continued to creep from the plateau with a similar timescale as the initial creep. This demonstrates that swelling occurred over the bulk of the material and not simply at the interface.

In confined environments, the dilatancy of stiff hydrogels under shear or sliding will lead to an increased normal force. To show this, we performed sliding experiments using a strain-controlled rheometer with PAA commercial hydrogel spheres, as depicted in the Fig. 2(b) inset. An aluminum plate (diameter = 60 mm) with three divots was

glued to the top parallel plate of the rheometer. The divots were placed at the vertices of an equilateral triangle, each 20 mm from the plate center. A small amount of modeling clay was used in the divots to prevent undesired rolling of the spheres. Sliding occurred at a smooth acrylic surface at the bottom of each sphere. An initial normal force of $F_0 = 0.9$ N was applied to compress the hydrogel spheres for 8 h. Subsequently, we applied a constant sliding velocity $v = 0.3$ cm/s to hydrogel spheres for ~13 h. Hydrogel spheres were monitored for 8 h post sliding. The gap size was constant throughout the experiment, corresponding to a normal strain of 3%. Upon initial compression, the normal force relaxed similarly to Fig. 1(a). During sliding ($8 < t < 21$ h), F_N initially increased by nearly 20% and eventually stabilized around the 16th hour. The post-sliding relaxation observed in Fig. 2(b) occurred over a similar timescale as the relaxation from the initial compression, providing further evidence of bulk, hyperelastic swelling during sliding.

Hyperelastic dilation from simple shear—To further show that the dilatant effects observed during sliding are a bulk property, we used oscillatory rheology to quantitatively investigate the strain dependence predicted in Eqs. (1) and (2). We fabricated PAAm disks of thickness 6 mm and diameter 60 mm. The hydrogel disks were fully immersed in deionized water and placed between acrylic plates affixed with sandpaper to ensure a large static friction, as illustrated in Fig. 3(a). The PAAm disks were initially compressed with a normal stress of ≈2–3 kPa, corresponding to a normal strain of 5%, and then relaxed for 14 h. Oscillatory strain sweep experiments were conducted over the range $0.006 \leq \gamma \leq 0.32$, spending 25 s per point. An oscillatory frequency of 1 Hz was chosen since it is much faster than the diffusive relaxation timescale. The change in normal stress, $\Delta\sigma_N$, is shown in Fig. 3(b) for multiple experiments and four different monomer concentrations. All data show remarkable agreement with $\Delta\sigma_N \propto \gamma^2$ [Eq. (1)] over more than a decade in strain. Using Eq. (1) and accounting for the average dilatant effect over the plate area [54], we found that R_v ranged from 13 to 538 kPa. This coefficient can be theoretically described by Eq. (2), which relies on Maxwell relations for the derivatives of elastic moduli in a hyperelastic material [43].

A hydrogel is necessarily more complex due to its poroelastic nature, i.e., there are time-dependent effects. Since the data from Fig. 3(b) start from a fully relaxed state of compression, we chose to measure the complex elastic shear modulus, $|G^*| = \sqrt{G'^2 + G''^2}$, and the Young's modulus, E, for fully relaxed hydrogels. The moduli of PAAm hydrogels can vary widely depending on cross-linker concentration and environmental conditions [63]. We choose a wide range of samples [Fig. 3(b)] to illustrate the robustness of shear-induced dilation. We found that across multiple samples, the data could be reasonably collapsed by normalizing $\Delta\sigma_N$ by $|G^*|$, which may be expected by the modulus dependency in Eq. (2). The collapse is shown in Fig. 3(c). Since $|G^*|$ can decrease with γ (Fig. S3), normalizing the data shifts their vertical position and also leads to a more consistent power law relationship, $\Delta\sigma_N/|G^*| \approx C\gamma^2/4$, where $C \approx 23.5$, as shown by the solid line.

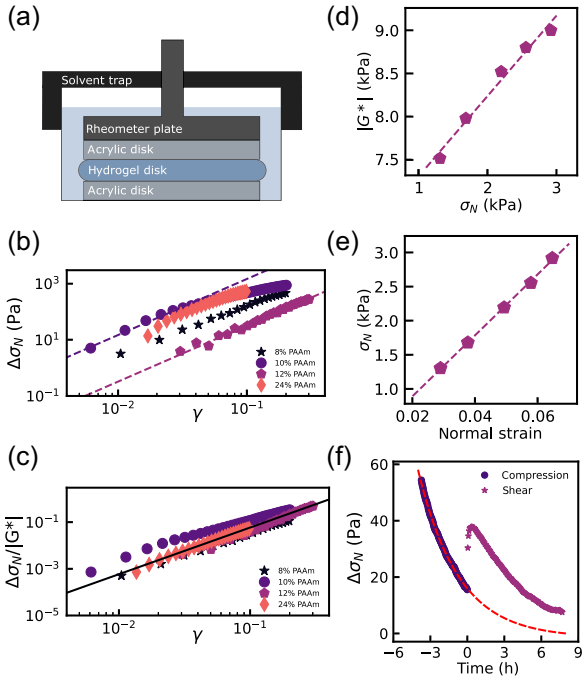

FIG. 3. Oscillatory rheology of hydrogels reveals a hyperelastic dilatancy. (a) Illustration showing a compressed PAAm disk of diameter 60 mm and thickness 6 mm between two acrylic disks affixed with sandpaper. Each hydrogel disk was compressed with an initial normal stress and allowed to relax prior to testing. (b) The change in normal stress ($\Delta\sigma_N$) vs strain (γ) for different hydrogel samples during an oscillatory strain sweep at 1 Hz. Each point is an average of 25 s spent at the corresponding strain. Dashed lines represent fitting results using the function $\Delta\sigma_N = R_v\gamma^2/4$ [Eq. (S8) [54]]. (c) By normalizing $\Delta\sigma_N$ using $|G^*|$ at each value of the strain (see Fig. S2), the data in panel (b) can be reasonably collapsed. The solid line represents $\Delta\sigma_N/|G^*| \approx 5.9\gamma^2$. (d) Complex modulus $|G^*|$ vs σ_N measured via oscillatory shear (1 Hz) at constant shear strain ($\gamma = 0.05$). (e) Normal stress versus normal strain. Young's modulus (E) can be calculated from the data [Eqs. (S5) and (S6) [54]]. For each point in (d),(e), the hydrogel was relaxed to equilibrium 3 h before testing, and the dashed lines represent linear fits. (f) $\Delta\sigma_N$ vs time for an 8% PAAm disk that was initially compressed to 2000 Pa. A subsequent period of shear stress ($\sigma_s = 150$ Pa) induced an increase in normal stress during the relaxation. The dashed line is an exponential fit to the relaxation period to estimate F_∞, which is used to determine $\Delta\sigma_N = 0$. During shear, the strain remained constant at ≈20%, indicating minimal slip at the hydrogel and sandpaper interfaces.

Figures 3(d) and 3(e) shows $|G^*|$ as a function of σ_N, and σ_N as a function of the normal strain for a 12% PAAm gel. Assuming a linear relationship for both, we extracted

$d|G^*|/d\sigma_N (\cong 0.93 \pm 0.076)$ and $E \cong 23.0 \pm 1.9$ kPa from the slopes of each fit, respectively. Errors were estimated from variation of linear fits in Figs. 3(d) and 3(e), respectively. To account for viscoelasticity, $|G^*|$ was used instead of G [34], and the measurement of E accounted for the no-slip boundary conditions on the confining parallel plates [Eq. (S5) [54,64]]. With these values, Eq. (2) estimates $R_v \cong 13.3 \pm 4.26$ kPa. This should be compared to 14.2 kPa for the 12% PAAm hydrogel shown in Fig. 3(b). The agreement is remarkable given that Eq. (2) relies solely on elastic energy [43], whereas the free energy of a hydrogel contains both elastic and mixing free energies [51,65].

Lastly, to demonstrate that this increase of $\Delta\sigma_N$ upon applied strain does not lead to an eventual negative normal stress as observed by de Cagny *et al.* [42] in low-modulus PAAm hydrogels, we compressed an 8% PAAm slab for 14 h, then applied a constant shear stress of 150 Pa for an additional 8 h, as shown in Fig. 3(f). We observed an exclusively positive normal stress response during this period, although concomitant with the continuing relaxation from compression. This further demonstrates that applied shear stress, regardless of the source, leads to a bulk dilational effect in stiff hydrogels.

Summary and outlook—We provided compelling evidence that stiff hydrogels exclusively dilate due to shear in both tribological and rheological experiments. The dilatancy was observed across short and long timescales and can be explained by the bulk, hyperelastic properties of hydrogels. Specifically, the measured Reynolds dilation coefficient (R_v) showed excellent agreement with leading order predictions from elasticity theory. Our results contradict prior experiments and theory suggesting purely contractile behavior in network materials and all hydrogels (provided sufficient time has elapsed for poroelastic relaxation). These results also provide an alternative explanation for the natural rehydration of stiff tissues such as cartilage during mechanical shearing, where dilation imbibes the surrounding synovial fluid. Although cartilage is more heterogeneous and complex than the hydrogels we investigated in this Letter (i.e., synovial fluid can be non-Newtonian), the fact that shear-induced swelling exists in both natural cartilage and simple stiff hydrogels suggests a more universal mechanism derived from the cross-linked network structure.

Given the contractile behavior observed in low-modulus gels, we expect the Reynolds coefficient R_v to change sign as the polymer network stiffens or softens. This transition should be related to the network microstructure and cross-linking density. Although purely elastic models such as random spring networks can capture many mechanical properties of hydrogel materials, they fail to capture shear-induced dilatancy [44]. While it is natural to assume that the amount of precompression (prestress) in hydrogels could affect their hyperelastic behavior, as expected in random spring networks, we did not see strong evidence of this in our experiments. We speculate that in dense, stiff, and highly cross-linked hydrogels, entropic effects encompassing both the crowded polymers and the solvent cannot be captured by a simple harmonic spring network. The relationship between hyperelasticity, poroelasticity, and hydrogel microstructure provides many open questions for future research. Finally, because stiff PAAm hydrogels are widely used for micromechanical measurements of cells and tissues (i.e., traction force microscopy [66–68]), we suggest that hyperelastic, shear-induced dilation should be considered when interpreting any data involving large deformations in stiff hydrogels.

Acknowledgments—We acknowledge Daniel Sussman for insightful conversations, and Eric Weeks for use of the rheometer. This work was supported by the Gordon and Betty Moore Foundation, Grant DOI 10.37807/gbmf12256.

[1] S. D. Palanivelu, N. A. Z. Armir, A. Zulkifli, A. H. A. Hair, K. M. Salleh, K. Lindsey, M. H. Che-Othman, and S. Zakaria, Hydrogel application in urban farming: Potentials and limitations–A review, Polymers **14**, 2590 (2022).
[2] S. Mitura, A. Sionkowska, and A. Jaiswal, Biopolymers for hydrogels in cosmetics, J. Mater. Sci. **31**, 1 (2020).
[3] M. Sachdev, Y. Anantheswar, B. Ashok, S. Hameed, and S. A. Pai, Facial granulomas secondary to injection of semi-permanent cosmetic dermal filler containing acrylic hydrogel particles, J. Cutaneous Aesthetic Surg. **3**, 162 (2010).
[4] K. Y. Lee and D. J. Mooney, Hydrogels for tissue engineering, Chem. Rev. **101**, 1869 (2001).
[5] J. L. Silverberg, A. R. Barrett, M. Das, P. B. Petersen, L. J. Bonassar, and I. Cohen, Structure-function relations and rigidity percolation in the shear properties of articular cartilage, Biophys. J. **107**, 1721 (2014).
[6] M. Hamidi, A. Azadi, and P. Rafiei, Hydrogel nanoparticles in drug delivery, Adv. Drug Delivery Rev. **60**, 1638 (2008).
[7] J. Li and D. J. Mooney, Designing hydrogels for controlled drug delivery, Nat. Rev. Mater. **1**, 1 (2016).
[8] C. A. Dreiss, Hydrogel design strategies for drug delivery, Curr. Opin. Colloid Interface Sci. **48**, 1 (2020).
[9] V. M. Sardinha, L. Lima, W. Belangero, C. Zavaglia, V. Bavaresco, and J. Gomes, Tribological characterization of polyvinyl alcohol hydrogel as substitute of articular cartilage, Wear **301**, 218 (2013).
[10] Y. A. Meier, K. Zhang, N. D. Spencer, and R. Simic, Linking friction and surface properties of hydrogels molded against materials of different surface energies, Langmuir **35**, 15805 (2019).
[11] M. Parkes, C. Myant, D. Dini, and P. Cann, Tribology-optimised silk protein hydrogels for articular cartilage repair, Tribol. Int. **89**, 9 (2015).
[12] M. M. Blum and T. C. Ovaert, Low friction hydrogel for articular cartilage repair: Evaluation of mechanical and tribological properties in comparison with natural cartilage tissue, Mater. Sci. Eng. C **33**, 4377 (2013).

[13] V. Bavaresco, C. Zavaglia, M. Reis, and J. Gomes, Study on the tribological properties of phema hydrogels for use in artificial articular cartilage, Wear **265**, 269 (2008).
[14] M. E. Freeman, M. J. Furey, B. J. Love, and J. M. Hampton, Friction, wear, and lubrication of hydrogels as synthetic articular cartilage, Wear **241**, 129 (2000).
[15] J. Kim and A. C. Dunn, Soft hydrated sliding interfaces as complex fluids, Soft Matter **12**, 6536 (2016).
[16] J. P. Gong, Friction and lubrication of hydrogels–its richness and complexity, Soft Matter **2**, 544 (2006).
[17] K. Vishwanath, S. R. McClure, and L. J. Bonassar, Polyacrylamide hydrogel lubricates cartilage after biochemical degradation and mechanical injury, J. Orthop. Res. **41**, 63 (2023).
[18] L. Han, J. Xu, X. Lu, D. Gan, Z. Wang, K. Wang, H. Zhang, H. Yuan, and J. Weng, Biohybrid methacrylated gelatin/polyacrylamide hydrogels for cartilage repair, J. Mater. Chem. B **5**, 731 (2017).
[19] D. L. Burris and A. C. Moore, Cartilage and joint lubrication: New insights into the role of hydrodynamics, Biotribology **12**, 8 (2017).
[20] D. Burris, L. Ramsey, B. Graham, C. Price, and A. Moore, How sliding and hydrodynamics contribute to articular cartilage fluid and lubrication recovery, Tribol. Lett. **67**, 1 (2019).
[21] M. S. Farnham, R. E. Larson, D. L. Burris, and C. Price, Effects of mechanical injury on the tribological rehydration and lubrication of articular cartilage, J. Mech. Behav. Biomed. Mater. **101**, 103422 (2020).
[22] C. Putignano, D. Burris, A. Moore, and D. Dini, Cartilage rehydration: The sliding-induced hydrodynamic triggering mechanism, Acta Biomater. **125**, 90 (2021).
[23] G. De Boer, N. Raske, S. Soltanahmadi, M. Bryant, and R. Hewson, Compliant-poroelastic lubrication in cartilage-on-cartilage line contacts, Tribol.-Mater. Surf. Interfaces **14**, 151 (2020).
[24] M. E. Kupratis, A. E. Gure, K. F. Ortved, D. L. Burris, and C. Price, Comparative tribology: Articulation-induced rehydration of cartilage across species, Biotribology **25**, 100159 (2021).
[25] A. C. Moore and D. L. Burris, Tribological rehydration of cartilage and its potential role in preserving joint health, Osteoarthritis Cartilage **25**, 99 (2017).
[26] J. Poynting, XXXIX. Radiation pressure, Philos. Mag. **9**, 393 (1905).
[27] J. H. Poynting, On pressure perpendicular to the shear planes in finite pure shears, and on the lengthening of loaded wires when twisted, Proc. R. Soc. A **82**, 546 (1909).
[28] E. Billington, The Poynting effect, Acta Mech. **58**, 19 (1986).
[29] E. Vitral, Stretch formulations and the Poynting effect in nonlinear elasticity, Int. J. Nonlinear Mech. **148**, 104293 (2023).
[30] C. Horgan and J. Murphy, Poynting and reverse Poynting effects in soft materials, Soft Matter **13**, 4916 (2017).
[31] C. Horgan and J. Murphy, The effect of fiber-matrix interaction on the Poynting effect for torsion of fibrous soft biomaterials, J. Mech. Behav. Biomed. Mater. **118**, 104410 (2021).
[32] J. L. Shivers, J. Feng, A. Sharma, and F. C. MacKintosh, Normal stress anisotropy and marginal stability in athermal elastic networks, Soft Matter **15**, 1666 (2019).
[33] S. Niroumandi, M. Shojaeifard, and M. Baghani, Finite deformation of swollen pH-sensitive hydrogel cylinder under extension and torsion and its Poynting effect: Analytical solution and numerical verification, Int. J. Appl. Mech. **13**, 2150071 (2021).
[34] A. Fall, B. P. Tighe, and D. Bonn, Tuneable normal stresses in hyperelastic emulsions, Phys. Rev. Res. **4**, 013167 (2022).
[35] M. Mooney, A theory of large elastic deformation, J. Appl. Phys. **11**, 582 (1940).
[36] R. S. Rivlin, Large elastic deformations of isotropic materials IV. Further developments of the general theory, Phil. Trans. R. Soc. A **241**, 379 (1948).
[37] P. A. Janmey, M. E. McCormick, S. Rammensee, J. L. Leight, P. C. Georges, and F. C. MacKintosh, Negative normal stress in semiflexible biopolymer gels, Nat. Mater. **6**, 48 (2007).
[38] H. Kang, Q. Wen, P. A. Janmey, J. X. Tang, E. Conti, and F. C. MacKintosh, Nonlinear elasticity of stiff filament networks: Strain stiffening, negative normal stress, and filament alignment in fibrin gels, J. Phys. Chem. B **113**, 3799 (2009).
[39] M. Vahabi, B. E. Vos, H. C. G. De Cagny, D. Bonn, G. H. Koenderink, and F. MacKintosh, Normal stresses in semiflexible polymer hydrogels, Phys. Rev. E **97**, 032418 (2018).
[40] E. Conti and F. C. MacKintosh, Cross-linked networks of stiff filaments exhibit negative normal stress, Phys. Rev. Lett. **102**, 088102 (2009).
[41] A. J. Licup, S. Münster, A. Sharma, M. Sheinman, L. M. Jawerth, B. Fabry, D. A. Weitz, and F. C. MacKintosh, Stress controls the mechanics of collagen networks, Proc. Natl. Acad. Sci. U.S.A. **112**, 9573 (2015).
[42] H. C. G. de Cagny, B. E. Vos, M. Vahabi, N. A. Kurniawan, M. Doi, G. H. Koenderink, F. C. MacKintosh, and D. Bonn, Porosity governs normal stresses in polymer gels, Phys. Rev. Lett. **117**, 217802 (2016).
[43] B. P. Tighe, Shear dilatancy in marginal solids, Granular Matter **16**, 203 (2014).
[44] K. Baumgarten and B. P. Tighe, Normal stresses, contraction, and stiffening in sheared elastic networks, Phys. Rev. Lett. **120**, 148004 (2018).
[45] O. Reynolds, Experiments showing dilatancy, a property of granular material, possibly connected with gravitation, Proc. R. Inst. Great Britain **11**, 12 (1886).
[46] M. Merkel, K. Baumgarten, B. P. Tighe, and M. L. Manning, A minimal-length approach unifies rigidity in underconstrained materials, Proc. Natl. Acad. Sci. U.S.A. **116**, 6560 (2019).
[47] J. P. Gong, Y. Katsuyama, T. Kurokawa, and Y. Osada, Double-network hydrogels with extremely high mechanical strength, Adv. Mater. **15**, 1155 (2003).
[48] J. P. Gong, Why are double network hydrogels so tough?, Soft Matter **6**, 2583 (2010).
[49] M. A. Haque, T. Kurokawa, and J. P. Gong, Super tough double network hydrogels and their application as biomaterials, Polymer **53**, 1805 (2012).

[50] K. Yasuda, J. P. Gong, Y. Katsuyama, A. Nakayama, Y. Tanabe, E. Kondo, M. Ueno, and Y. Osada, Biomechanical properties of high-toughness double network hydrogels, Biomaterials **26**, 4468 (2005).
[51] M. Doi, Gel dynamics, J. Phys. Soc. Jpn. **78**, 052001 (2009).
[52] M. Doi and S. Edwards, Dynamics of concentrated polymer systems. Part 1. Brownian motion in the equilibrium state, J. Chem. Soc., Faraday Trans. 2 **74**, 1789 (1978).
[53] J.-F. Louf and S. S. Datta, Poroelastic shape relaxation of hydrogel particles, Soft Matter **17**, 3840 (2021).
[54] See Supplemental Material at http://link.aps.org/supplemental/10.1103/PhysRevLett.134.148203 for further details of the experimental methods and analysis.
[55] N. L. Cuccia, S. Pothineni, B. Wu, J. Méndez Harper, and J. C. Burton, Pore-size dependence and slow relaxation of hydrogel friction on smooth surfaces, Proc. Natl. Acad. Sci. U.S.A. **117**, 11247 (2020).
[56] J. D. Berry, M. Biviano, and R. R. Dagastine, Poroelastic properties of hydrogel microparticles, Soft Matter **16**, 5314 (2020).
[57] Y. Hu, X. Zhao, J. J. Vlassak, and Z. Suo, Using indentation to characterize the poroelasticity of gels, Appl. Phys. Lett. **96** (2010).
[58] Z. I. Kalcioglu, R. Mahmoodian, Y. Hu, Z. Suo, and K. J. Van Vliet, From macro-to microscale poroelastic characterization of polymeric hydrogels via indentation, Soft Matter **8**, 3393 (2012).
[59] S. Cuenot, P. Gélébart, C. Sinquin, S. Colliec-Jouault, and A. Zykwinska, Mechanical relaxations of hydrogels governed by their physical or chemical crosslinks, J. Mech. Behav. Biomed. Mater. **133**, 105343 (2022).
[60] M. H. Esteki, A. A. Alemrajabi, C. M. Hall, G. K. Sheridan, M. Azadi, and E. Moeendarbary, A new framework for characterization of poroelastic materials using indentation, Acta Biomater. **102**, 138 (2020).
[61] J. Crank, *The Mathematics of Diffusion* (Oxford University Press, New York, 1979).
[62] B. Wu, J. M. Harper, and J. C. Burton, Relaxation and recovery in hydrogel friction on smooth surfaces, Exp. Mech. **61**, 1081 (2021).
[63] A. K. Denisin and B. L. Pruitt, Tuning the range of polyacrylamide gel stiffness for mechanobiology applications, ACS Appl. Mater. Interfaces **8**, 21893 (2016).
[64] J. Williams and C. Gamonpilas, Using the simple compression test to determine Young's modulus, Poisson's ratio and the Coulomb friction coefficient, Int. J. Solids Struct. **45**, 4448 (2008).
[65] P. J. Flory and J. Rehner Jr, Statistical mechanics of cross-linked polymer networks II. Swelling, J. Chem. Phys. **11**, 521 (1943).
[66] M. Dembo and Y.-L. Wang, Stresses at the cell-to-substrate interface during locomotion of fibroblasts, Biophys. J. **76**, 2307 (1999).
[67] J. P. Butler, I. M. Tolic-Nørrelykke, B. Fabry, and J. J. Fredberg, Traction fields, moments, and strain energy that cells exert on their surroundings, Am. J. Physiol. **282**, C595 (2002).
[68] S. R. Polio, K. E. Rothenberg, D. Stamenović, and M. L. Smith, A micropatterning and image processing approach to simplify measurement of cellular traction forces, Acta Biomater. **8**, 82 (2012).